Modification and expansion of the generalized soft-sphere model to high temperature based on collision integrals

Jae Gang Kim, Oh Joon Kwon,[a] and Chul Park
Department of Aerospace Engineering, Korea Advanced Institute of Science and Technology, Daejeon 305-701, Republic of Korea

(Received 14 June 2007; accepted 30 November 2007; published online 23 January 2008)

In the present study, modification and expansion of the collision parameters for the general soft-sphere model [J. Fan, Phys. Fluids **12**, 4399 (2002)] were made for use in the direct simulation Monte Carlo calculation of hypersonic flows in the temperature range of 300–50 000 K. The collision integrals were expressed as a two-term function in a form of the inverse power of temperature, which was cast in terms of the soft-sphere scattering parameters and the four total cross-section parameters. Next, the most recent available data for the diffusion and viscosity collision integrals were collected and fitted into a function of temperature in the same form. By equating these expressions for the diffusion and viscosity collision integrals simultaneously, the five collision parameters were deduced as functions of species combinations. The resulting collision parameters for the general soft-sphere model were tabulated for 191 collision pairs involving 22 species. It was shown that the transport properties calculated by using the present collision parameters are much closer to experiments, theoretical data, and the values obtained by the *ab initio* calculations from quantum-mechanically derived potential energy surfaces than existing elastic collision models. The direct simulation Monte Carlo calculation of flow around a circular cylinder confirmed that discernible differences exist between the results based on the present study and those of the existing models. © *2008 American Institute of Physics*. [DOI: 10.1063/1.2832781]

I. INTRODUCTION

Several different mathematical models have been previously developed for the description of the elastic collision in the direct simulation Monte Carlo (DSMC) calculation of hypersonic rarefied gas flows. The latest one among them is the generalized soft-sphere (GSS) model[1] in which the total cross section is defined to be identical to that of the generalized hard-sphere (GHS) model[2,3] introduced earlier, while the deflection angle is set the same as in the soft-sphere scattering model. In the GSS model, a two-term formula is used for the evaluation of the reduced viscosity collision integral of the Lennard-Jones (LJ) 6-12 potential and the Stockmayer potential.[4] It is known that up to 2000 K, the viscosity and diffusion coefficients of the GSS model are in better agreement with experimental values than the other previous models. Another elastic collision model is the variable soft-sphere (VSS) model,[5,6] in which the deflection angle is determined based on the soft-sphere assumption and the collision parameters are evaluated by the inverse power law (IPL) model and the LJ potential.

However, in the GSS model, the scattering parameter is fixed as a constant, and as a result, the reduced diffusion and viscosity collision integrals, $\Omega^{(1,1)^*}$ and $\Omega^{(2,2)^*}$, are not accurately reproduced. In Fig. 1, the discrepancy of the collision integrals between the values calculated by the GSS model and the LJ potential is presented. Because the reduced viscosity collision integral was used as the basis for the derivation, the values of the two models match closely. However, for the other collision integrals, the discrepancies are approximately three times larger than that of the reduced viscosity collision integral. Meanwhile, in the variable soft-sphere (VSS) model, the scattering parameter is treated as a species-dependent value, and thus the reduced diffusion and viscosity collision integrals are reproduced more accurately.

There is another limitation to the usage of the GSS model. The GSS model relies on the LJ and Stockmayer potentials which mostly account for the long-range attraction that is dominant at relatively low temperatures. But at high temperatures, short-range repulsive forces are dominant, and therefore the LJ potential becomes inaccurate. Also, the interaction potentials caused by the collisions among molecules, atoms, and charged particles are very much different from the LJ and Stockmayer potentials. In Fig. 2, it is shown that the collision integrals derived from the LJ potential are substantially different from those obtained from the *ab initio* calculations[7,8] based on the quantum-mechanically derived potential energy surfaces.

In the present study, an improvement was made to the GSS model so that the elastic collisions of atoms, molecules, and charged particles can be described better at high temperatures. For this purpose, the total cross section and the soft-sphere assumption were still used, but the scattering parameter was taken to be implicitly species-dependent as in the VSS model. The collision parameters for the neutral and charged particles were determined by adopting the best available diffusion and viscosity collision integrals, which were taken simultaneously from the most recent and physically adequate data obtained either by the *ab initio* calculations[7–17]

[a]Author to whom correspondence should be addressed. Telephone: +82-42-869-3720. Fax: +82-42-869-3710. Electronic mail: ojkwon@kaist.ac.kr.

 © 2008 American Institute of Physics

Downloaded 19 Apr 2011 to 143.248.103.97. Redistribution subject to AIP license or copyright; see http://pof.aip.org/about/rights_and_permissions

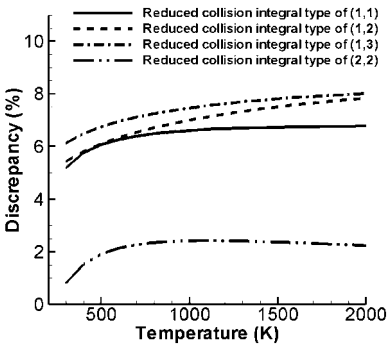

FIG. 1. Discrepancy of the reduced collision integrals between the GSS model and the LJ potential.

from the quantum-mechanically derived potential energy surfaces, from the experiments,[18] or from the theory.[19–23] The accuracy of the present method was validated by comparing the values of the collision integrals, $\bar{\Omega}^{(1,2)}$ and $\bar{\Omega}^{(1,3)}$, with those obtained from the *ab initio* calculations. The transport properties calculated by the present collision parameters were also compared with experimental values, reference transport properties based on the best collision integrals, and the previous elastic collision models. For a demonstration, a DSMC calculation for flow around a circular cylinder was made for N_2 and NO species using the present collision parameters, and the results were compared with those obtained by previous elastic collision models.

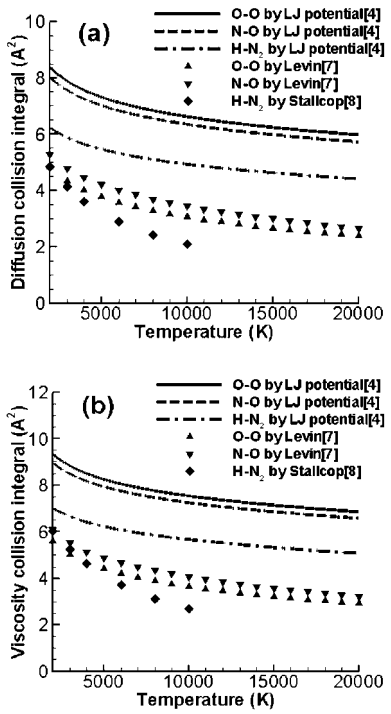

FIG. 2. Comparison of the collision integrals between the LJ potential (Ref. 4) and the *ab initio* calculations (Refs. 7 and 8). (a) Diffusion collision integral; (b) viscosity collision integral.

II. MODIFICATION AND EXPANSION OF THE GSS MODEL

The GSS model is based on the soft-sphere assumption characterized by the scattering parameter α in the form

$$b = d\cos^{\alpha}\left(\frac{\chi}{2}\right), \tag{1}$$

where b, d, and χ are the impact parameter, the variable diameter, and the scattering angle, respectively. To describe the cross section, the GSS model adopts the same formulation as in the GHS model,

$$\frac{\sigma_T}{\sigma^2} = \sum_{j=1}^{2} \zeta_j \left(\frac{E}{\varepsilon}\right)^{-\xi_j}, \tag{2}$$

where σ is the diameter of the collision molecule, and ε is the potential-energy well depth. Also, E is the impact energy, and the collision parameters, ζ_1, ζ_2, ξ_1, ξ_2 and α, are the unknown variables for the total cross-section σ_T and the scattering angle χ.

The reduced momentum and viscous cross sections, $\Omega^{(1)^*}$ and $\Omega^{(2)^*}$, can be written as[4]

$$\Omega^{(\ell)*} = \frac{2}{1-\frac{1}{2}\left(\frac{1+(-1)^{-\ell}}{1+\ell}\right)} \int_0^{\infty} (1-\cos^{\ell}\chi) b^* db^*, \tag{3}$$

where ℓ is the index for the cross section, and the superscript $*$ denotes the reduced value quantity. In the present study, the reduced cross sections for momentum and viscosity were recast by using Eqs. (1)–(3) as

$$\Omega^{(1)*}(g^*) = \frac{2}{\pi(\alpha+1)} \sum_{j=1}^{2} \zeta_j (g^*)^{-2\xi_j}, \tag{4}$$

$$\Omega^{(2)*}(g^*) = \frac{6\alpha}{\pi(\alpha+1)(\alpha+2)} \sum_{j=1}^{2} \zeta_j (g*)^{-2\xi_j}, \tag{5}$$

where g^* denotes the reduced relative impact energy. According to the Chapman–Enskog theory,[4] the collision integrals are defined as

$$\Omega^{(\ell,s)*}(T^*) = \frac{2}{(s+1)!T^{*s+2}} \int_0^{\infty} \exp\left(-\frac{g^{*2}}{T^*}\right) \times g^{*2s+3} \Omega^{(\ell)*}(g^*) dg^*, \tag{6}$$

where T^* is the reduced temperature. Using Eqs. (4)–(6), the collision integrals can be rewritten as

$$\bar{\Omega}^{(1,1)} = \sigma^2 \Omega^{(1,1)^*}(T^*) = \sum_{j=1}^{2} \frac{\sigma^2 \zeta_j}{\pi(\alpha+1)} \Gamma(3-\xi_j)(T^*)^{-\xi_j}, \tag{7}$$

$$\bar{\Omega}^{(1,2)} = \sigma^2 \Omega^{(1,2)^*}(T^*) = \sum_{j=1}^{2} \frac{\sigma^2 \zeta_j}{3\pi(\alpha+1)} \Gamma(4-\xi_j)(T^*)^{-\xi_j}, \tag{8}$$

Downloaded 19 Apr 2011 to 143.248.103.97. Redistribution subject to AIP license or copyright; see http://pof.aip.org/about/rights_and_permissions

$$\bar{\Omega}^{(1,3)} = \sigma^2 \Omega^{(1,3)^*}(T^*) = \sum_{j=1}^{2} \frac{\sigma^2 \zeta_j}{12\pi(\alpha+1)} \Gamma(5-\xi_j)(T^*)^{-\xi_j}, \tag{9}$$

$$\bar{\Omega}^{(2,2)} = \sigma^2 \Omega^{(2,2)^*}(T^*) = \sum_{j=1}^{2} \frac{\sigma^2 \alpha \zeta_j}{\pi(\alpha+1)(\alpha+2)} \Gamma(4-\xi_j)(T^*)^{-\xi_j}. \tag{10}$$

The collision parameters, ζ_1, ζ_2, ξ_1, ξ_2 and α, have nonlinear dependencies on each other, and thus to determine these parameters, the collision integrals, $\bar{\Omega}^{(1,1)}$ and $\bar{\Omega}^{(2,2)}$, need to be solved simultaneously.

Cubley and Mason[18] have fitted the experimentally determined collision integrals as a function of the inverse power of temperature. In the present study, it was proposed that the diffusion collision integral $\bar{\Omega}^{(1,1)}$ is fitted as a two-term function which is composed of the inverse power of temperature, same to the existing GSS model,

$$\bar{\Omega}^{(1,1)} = \psi_1^{(1,1)} \left(\frac{10000}{T} \right)^{\psi_2^{(1,1)}} + \psi_3^{(1,1)} \left(\frac{10000}{T} \right)^{\psi_4^{(1,1)}}. \tag{11}$$

The parameters, $\psi_1^{(1,1)}$, $\psi_2^{(1,1)}$, $\psi_3^{(1,1)}$, and $\psi_4^{(1,1)}$, in Eq. (11) can be determined by applying the nonlinear least-square regression to the best available diffusion collision integrals. By equating Eqs. (7) and (11), the diffusion collision integral is

$$\bar{\Omega}^{(1,1)} = \psi_1^{(1,1)} \left(\frac{10000}{T} \right)^{\psi_2^{(1,1)}} + \psi_3^{(1,1)} \left(\frac{10000}{T} \right)^{\psi_4^{(1,1)}} = \sum_{j=1}^{2} \frac{\sigma^2 \zeta_j}{\pi(\alpha+1)} \Gamma(3-\xi_j) \left(\frac{kT}{\varepsilon} \right)^{-\xi_j}. \tag{12}$$

Then the collision parameters, ξ_1 and ξ_2, can be set as $\xi_1 = \psi_2^{(1,1)}$ and $\xi_1 = \psi_4^{(1,1)}$. However, because the parameter α is not known, the collision parameters, ζ_1 and ζ_2, cannot be determined. In the present study, to determine the collision parameters, ξ_1 and ξ_2, the viscosity collision integral $\bar{\Omega}^{(2,2)}$ was used. From Eqs. (7), (10), and (12), the viscosity collision integral $\bar{\Omega}^{(2,2)}$ can be rewritten as

$$\bar{\Omega}^{(2,2)} = \frac{\alpha}{\alpha+2} \frac{\Gamma(4-\xi_1)}{\Gamma(3-\xi_1)} \psi_1^{(1,1)} \left(\frac{10000}{T} \right)^{\psi_2^{(1,1)}} + \frac{\alpha}{\alpha+2} \frac{\Gamma(4-\xi_2)}{\Gamma(3-\xi_2)} \psi_3^{(1,1)} \left(\frac{10000}{T} \right)^{\psi_4^{(1,1)}}. \tag{13}$$

Since the viscosity collision integral $\bar{\Omega}^{(2,2)}$ is only a function of the scattering parameter α, the scattering parameter can be determined by applying the linear least-square regression to the best available viscosity collision integrals. Then from this scattering parameter α and Eqs. (7) and (10), the collision parameters, ζ_1 and ζ_2, can be formulated as

$$\zeta_1 = \frac{\psi_1^{(2,2)} (10000)^{\xi_1} \pi(\alpha+1)(\alpha+2)}{\sigma^2 \alpha \Gamma(4-\xi_1)} \left(\frac{k}{\varepsilon} \right)^{\xi_1}, \tag{14}$$

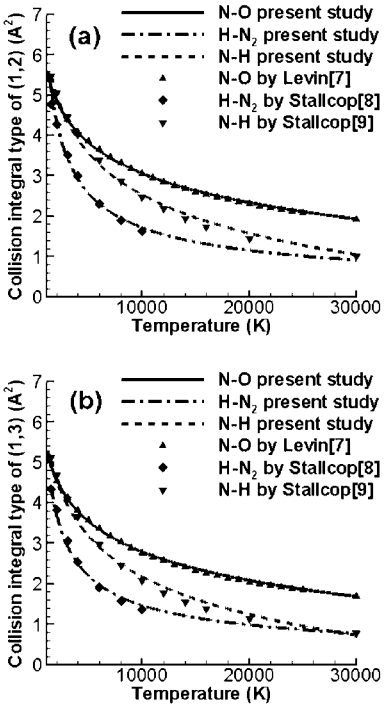

FIG. 3. Comparison of collision integrals between the present study and the *ab initio* calculations (Refs. 7–9). (a) Collision integral type of (1,2); (b) collision integral type of (1,3).

$$\zeta_2 = \frac{\psi_3^{(2,2)} (10000)^{\xi_2} \pi(\alpha+1)(\alpha+2)}{\sigma^2 \alpha \Gamma(4-\xi_2)} \left(\frac{k}{\varepsilon} \right)^{\xi_2}, \tag{15}$$

where $\psi_1^{(2,2)}$ and $\psi_3^{(2,2)}$ are given as

$$\psi_1^{(2,2)} = \frac{\alpha}{\alpha+2} \frac{\Gamma(4-\xi_1)}{\Gamma(3-\xi_1)} \psi_1^{(1,1)}, \tag{16}$$

$$\psi_3^{(2,2)} = \frac{\alpha}{\alpha+2} \frac{\Gamma(4-\xi_2)}{\Gamma(3-\xi_2)} \psi_3^{(1,1)}. \tag{17}$$

In order to verify the above procedure for determining the collision parameters, the collision integrals, $\bar{\Omega}^{(1,2)}$ and $\bar{\Omega}^{(1,3)}$, determined from Eqs. (8) and (9) were compared with the known values which were obtained from the *ab initio* calculations for N–O,[7] H–N_2,[8] and N–H.[9] In Fig. 3, it is shown that the collision integrals, $\bar{\Omega}^{(1,2)}$ and $\bar{\Omega}^{(1,3)}$, obtained from the present study agree very closely with those of the *ab initio* calculations.

III. DETERMINATION OF COLLISION PARAMETERS

When the collision parameters are to be determined, information about the collision integrals is needed. In the present study, to provide this information, all available data about the binary collision integrals were reassessed whenever available. A preference was given to the collision integrals obtained by the *ab initio* calculations[7–17] from quantum-mechanically derived potential energy surfaces. However, since these *ab initio* calculations have been made only for a limited number of collision pairs, the collision integrals for other collision pairs were collected from

Downloaded 19 Apr 2011 to 143.248.103.97. Redistribution subject to AIP license or copyright; see http://pof.aip.org/about/rights_and_permissions

experiments,[18] theoretical data,[19–23] and compilations.[24–27]

For neutral-neutral interactions, some collision integrals were evaluated by using the *ab initio* calculations.[7–15] In the case of those collisions for which such calculations were not available, experimental and theoretical data, such as the high fidelity potentials obtained by Murphy and Arundell[19] based on the data by Cubley and Mason,[18] the universal collision integrals obtained by Bzowski *et al.*,[20] and the compilations by Park, Jaffe, and Partridge,[24] Wright *et al.*,[25] Capitelli *et al.*,[26] and Gupta *et al.*,[27] were used.

For charge-neutral interactions, the *ab initio* calculations for the collision integrals have been made by Stallcop and Partridge.[16,17] When such calculations were not made, the collision integrals were obtained as either resonant or nonresonant collisions. In the case of the resonant collisions, the charge transfer cross sections[21,22] and the polarizability model[27] were considered. For the nonresonant collisions, the polarizability model[27] was adopted.

There are collision pairs for which the collision integrals are not known. For these collisions, estimated collision integrals were used. For neutral-neutral interactions, Park, Jaffe, and Partridge proposed a modified Lennard-Jones model,[24]

$$\bar{\Omega}^{(\ell,s)} = 0.9\bar{\Omega}^{(\ell,s)}_{\mathrm{LJ}}(T/2000)^{-0.25} \tag{18}$$

where the subscript LJ represents the Lennard-Jones 6-12 potential, and the superscript (ℓ,s) stands for the type of the collision integral. It is known that the modified LJ model in Eq. (18) agrees fairly well with the *ab initio* calculations at high temperatures. In the present study, this modified LJ model was used for calculating the unknown collision integrals.

The new collision parameters of the GSS model, ζ_1, ζ_2, ξ_1, ξ_2 and α, were calculated for 22 species, N_2, O_2, NO, CO, CO_2, C_2, H_2, CN, CH_4, He, Ar, N, O, C, H, N_2^+, O_2^+, NO^+, N^+, O^+, C^+ and H^+, and 191 collision pairs. The calculations were made by using all available sources about the collision integrals within 2% accuracy. The total cross section in Eq. (2) can be rewritten in a more convenient form as

$$\sigma_T = C_1 E^{\omega_1} + C_2 E^{\omega_2}. \tag{19}$$

In Table I, the total cross-section parameters, C_1, C_2, ω_1, and ω_2, and the scattering parameter α of the neutral-neutral and neutral-ion interactions are presented in the temperature range of 300–50 000 K.

IV. EVALUATION OF TRANSPORT PROPERTIES

Using Eqs. (7) and (10), the viscosity and diffusion coefficients can be derived by following the Chapman–Enskog procedure:[4]

$$\eta_{12} = 2.6693 \times 10^{-5} \frac{\pi(\alpha+1)(\alpha+2)\sqrt{2M_1M_2T/(M_1+M_2)}}{\sigma_{12}\alpha\Sigma_{j=1}^{2}\zeta_j\Gamma(4-\xi_j)(T_{12}^*)^{-\xi_j}}, \tag{20}$$

$$D_{12} = 2.628 \times 10^{-3} \frac{\pi(\alpha+1)\sqrt{T^3(M_1+M_2)/2M_1M_2}}{\sigma_{12}\Sigma_{j=1}^{2}\zeta_j\Gamma(3-\xi_j)(T_{12}^*)^{-\xi_j}}, \tag{21}$$

where the subscripts 1 and 2 are the species index. Also, $\sigma_{12}=(\sigma_1+\sigma_2)/2$ and $\varepsilon_{12}=\sqrt{\varepsilon_1\varepsilon_2}$. η_{12} and D_{12} are the viscosity and diffusion coefficients, respectively.

Maitland and Smith[28] reassessed the available viscosity coefficients which were obtained experimentally for common species, and recommended the values suitable in the temperature range of 20–2000 K. Comparison of the viscosity coefficients between the present study and the experimental values[28] for N_2, O_2, H_2, and Ar is presented in Fig. 4. It shows that in the temperature range of 300–2000 K, the transport properties calculated by Eq. (20) with the new collision parameters agree very well with the experimental values. In the case of the diffusion coefficients, the experimental data is not available for validation for the temperatures above 300 K. However, since the collision parameters in the present study were determined by using the diffusion and viscosity collision integrals, $\bar{\Omega}^{(1,1)}$ and $\bar{\Omega}^{(2,2)}$, simultaneously, the accuracy of the diffusion coefficients can also be assured.

For the molecule-molecule collisions, the transport properties calculated by Eqs. (20) and (21) with the new collision parameters were validated by comparing the results with those calculated from the VSS and GSS models and also with the reference values which were obtained by either the *ab initio* calculations[10,14] or the theoretical data.[19,20] When calculating the transport properties of the VSS and GSS models, the collision parameters are needed for each collision model. For the VSS model, the collision parameters[6] have been calculated for N_2, O_2, and NO based on the work by Cubley and Mason.[18] These collision parameters are valid in the temperature range of 300–16 000 K. For other species, they were determined from the IPL model and the LJ potential. For the GSS model, the collision parameters[1] have been calculated from the collision integrals obtained by the LJ potential.[4]

In Figs. 5 and 6, the transport properties for N_2–N_2 and N_2–H_2 collisions calculated by the present study are compared with the reference values obtained by the *ab initio* calculations[10] and those calculated from the VSS and GSS models. It shows that the difference between the present study and the reference values is quite small for both viscosity and diffusion coefficients. The results of the VSS model showed a significant difference from the reference values, particularly for N_2–H_2 collisions.

In Fig. 7, comparisons of the transport properties were made for the NO–NO collision. It is shown that the transport properties from the present study and the VSS model agree closely with the reference values obtained by the theoretical data, whereas a significant deviation was observed for the GSS model at high temperatures. This discrepancy of the transport properties between the GSS model and the reference values indicates that the extrapolation of the LJ potential is inadequate to describe the collisions as the temperature increases.

In Fig. 8, the transport properties by the present study for

Downloaded 19 Apr 2011 to 143.248.103.97. Redistribution subject to AIP license or copyright; see http://pof.aip.org/about/rights_and_permissions

TABLE I. Elastic collision parameters, total cross section parameters, C_1, C_2, ω_1, and ω_2, and the scattering parameter α for the temperature range of 300–50 000 K.

Species	C_1	C_2	ω_1	ω_2	α	Source
N_2-N_2	$-0.8706\times10^{+05}$	$0.1834\times10^{+00}$	$0.2281\times10^{+00}$	$-0.1192\times10^{+00}$	1.3629	Ref. 11
N_2-O_2	$-0.2778\times10^{+02}$	0.9789×10^{-01}	0.3032×10^{-01}	$-0.1306\times10^{+00}$	1.3869	Ref. 19
N_2-NO	$-0.4513\times10^{+03}$	$0.1107\times10^{+00}$	0.7999×10^{-01}	$-0.1358\times10^{+00}$	1.4706	Ref. 20
N_2-CO	-0.1466×10^{-03}	0.8456×10^{-03}	$-0.2424\times10^{+00}$	$-0.2423\times10^{+00}$	1.4138	Present study
N_2-CO_2	-0.6522×10^{-04}	0.9539×10^{-03}	$-0.2398\times10^{+00}$	$-0.2401\times10^{+00}$	1.4060	Present study
N_2-C_2	-0.9683×10^{-04}	0.7775×10^{-03}	$-0.2445\times10^{+00}$	$-0.2445\times10^{+00}$	1.4187	Present study
N_2-H_2	$-0.1362\times10^{+05}$	$0.1814\times10^{+00}$	$0.1728\times10^{+00}$	$-0.1159\times10^{+00}$	1.4763	Ref. 11
N_2-CN	$0.0000\times10^{+00}$	$0.5652\times10^{+03}$	$0.0000\times10^{+00}$	$-0.2473\times10^{+00}$	1.4198	Present study
N_2-CH_4	0.1065×10^{-02}	0.2083×10^{-29}	$-0.2345\times10^{+00}$	$-0.1539\times10^{+01}$	1.4103	Present study
N_2-He	-0.4981×10^{-01}	0.9532×10^{-04}	$-0.1210\times10^{+00}$	$-0.2868\times10^{+00}$	1.6109	Present study
N_2-Ar	$-0.1476\times10^{+07}$	$0.8010\times10^{+07}$	$0.2912\times10^{+00}$	-0.8268×10^{-01}	1.3678	Ref. 19
N_2-N	$-0.2302\times10^{+02}$	0.8721×10^{-03}	0.2928×10^{-01}	$-0.2410\times10^{+00}$	1.7826	Ref. 12
N_2-O	$-0.4599\times10^{+02}$	$0.2385\times10^{+00}$	0.3723×10^{-01}	$-0.1081\times10^{+00}$	1.3624	Ref. 19
N_2-C	-0.4544×10^{-18}	0.5226×10^{-07}	$-0.9960\times10^{+00}$	$-0.4605\times10^{+00}$	1.5899	Ref. 24
N_2-H	0.7205×10^{-60}	0.1915×10^{-09}	$-0.3041\times10^{+01}$	$-0.5800\times10^{+00}$	2.1333	Ref. 12
$N_2-N_2^+$	$0.8640\times10^{+02}$	0.1086×10^{-07}	0.1739×10^{-01}	$-0.4877\times10^{+00}$	0.2899	Ref. 21
$N_2-O_2^+$	$0.2042\times10^{+00}$	0.4770×10^{-20}	$-0.1016\times10^{+00}$	$-0.1120\times10^{+01}$	1.7238	Ref. 27
N_2-NO^+	0.8194×10^{-09}	0.1001×10^{-05}	$0.1680\times10^{+00}$	$-0.4000\times10^{+00}$	1.1039	Ref. 27
N_2-N^+	0.1779×10^{-16}	0.1001×10^{-05}	$-0.3202\times10^{+00}$	$-0.4000\times10^{+00}$	1.1039	Ref. 27
N_2-O^+	0.8194×10^{-09}	0.1001×10^{-05}	$0.1680\times10^{+00}$	$-0.4000\times10^{+00}$	1.1039	Ref. 27
N_2-C^+	$-0.2175\times10^{+43}$	0.1116×10^{-05}	$0.2407\times10^{+01}$	$-0.3978\times10^{+00}$	1.1100	Ref. 24
N_2-H^+	$-0.4910\times10^{+30}$	0.1289×10^{-05}	$0.1682\times10^{+01}$	$-0.3945\times10^{+00}$	1.1097	Ref. 24
O_2-O_2	$-0.4377\times10^{+00}$	$0.3273\times10^{+00}$	$-0.1358\times10^{+00}$	$-0.1458\times10^{+00}$	1.4333	Ref. 20
O_2-NO	$-0.3608\times10^{+01}$	0.3551×10^{-01}	-0.2894×10^{-01}	$-0.1606\times10^{+00}$	1.4637	Ref. 20
O_2-CO	-0.2529×10^{-03}	0.9142×10^{-03}	$-0.2421\times10^{+00}$	$-0.2421\times10^{+00}$	1.4131	Present study
O_2-CO_2	-0.1711×10^{-03}	0.1010×10^{-02}	$-0.2400\times10^{+00}$	$-0.2400\times10^{+00}$	1.4053	Present study
O_2-C_2	-0.5433×10^{-04}	0.7028×10^{-03}	$-0.2441\times10^{+00}$	$-0.2441\times10^{+00}$	1.4180	Present study
O_2-H_2	0.4424×10^{-03}	$0.0000\times10^{+00}$	$-0.2451\times10^{+00}$	$0.0000\times10^{+00}$	1.4189	Present study
O_2-CN	0.6858×10^{-03}	-0.4092×10^{-73}	$-0.2430\times10^{+00}$	$-0.3726\times10^{+01}$	1.4197	Present study
O_2-CH_4	-0.1337×10^{-03}	0.8949×10^{-03}	$-0.2410\times10^{+00}$	$-0.2410\times10^{+00}$	1.4099	Present study
O_2-He	$-0.2962\times10^{+07}$	0.1368×10^{-05}	$0.3633\times10^{+00}$	$-0.3720\times10^{+00}$	1.6128	Present study
O_2-Ar	$-0.3190\times10^{+05}$	$0.2334\times10^{+00}$	$0.1978\times10^{+00}$	$-0.1120\times10^{+00}$	1.4104	Ref. 19
O_2-N	-0.5969×10^{-02}	0.7193×10^{-01}	0.4292×10^{-01}	$-0.1373\times10^{+00}$	1.5086	Ref. 26
O_2-O	$-0.3024\times10^{+02}$	0.5280×10^{-01}	0.2582×10^{-01}	$-0.1449\times10^{+00}$	1.4784	Ref. 12
O_2-C	0.2578×10^{-07}	0.3785×10^{-06}	$-0.4078\times10^{+00}$	$-0.4078\times10^{+00}$	1.5767	Ref. 24
O_2-H	$-0.1461\times10^{+11}$	0.8207×10^{-06}	$0.5926\times10^{+00}$	$-0.3870\times10^{+00}$	1.5789	Ref. 12
$O_2-N_2^+$	0.8194×10^{-09}	0.1001×10^{-05}	$0.1680\times10^{+00}$	$-0.4000\times10^{+00}$	1.1039	Ref. 27
$O_2-O_2^+$	0.6227×10^{-01}	$0.1687\times10^{+00}$	$-0.1248\times10^{+00}$	$-0.1248\times10^{+00}$	0.1112	Ref. 22
O_2-NO^+	0.8194×10^{-09}	0.1001×10^{-05}	$0.1680\times10^{+00}$	$-0.4000\times10^{+00}$	1.1039	Ref. 27
O_2-N^+	0.8194×10^{-09}	0.1001×10^{-05}	$0.1680\times10^{+00}$	$-0.4000\times10^{+00}$	1.1039	Ref. 27
O_2-O^+	0.8194×10^{-09}	0.1001×10^{-05}	$0.1680\times10^{+00}$	$-0.4000\times10^{+00}$	1.1039	Ref. 27
O_2-C^+	$-0.4909\times10^{+30}$	0.1289×10^{-05}	$0.1682\times10^{+01}$	$-0.3945\times10^{+00}$	1.1097	Ref. 24
O_2-H^+	$-0.4910\times10^{+30}$	0.1289×10^{-05}	$0.1682\times10^{+01}$	$-0.3945\times10^{+00}$	1.1097	Ref. 24
NO–NO	$-0.1705\times10^{+02}$	0.4316×10^{-01}	0.4348×10^{-02}	$-0.1572\times10^{+00}$	1.4888	Ref. 20
NO–CO	-0.2400×10^{-03}	0.9284×10^{-03}	$-0.2416\times10^{+00}$	$-0.2416\times10^{+00}$	1.4116	Present study
$NO-CO_2$	-0.1445×10^{-03}	0.1007×10^{-02}	$-0.2398\times10^{+00}$	$-0.2398\times10^{+00}$	1.4038	Present study
$NO-C_2$	-0.7784×10^{-04}	0.7581×10^{-03}	$-0.2434\times10^{+00}$	$-0.2434\times10^{+00}$	1.4164	Present study
$NO-H_2$	-0.3120×10^{-03}	0.7575×10^{-03}	$-0.2454\times10^{+00}$	$-0.2454\times10^{+00}$	1.4205	Present study
NO–CN	-0.7885×10^{-04}	0.7372×10^{-03}	$-0.2437\times10^{+00}$	$-0.2437\times10^{+00}$	1.4171	Present study
$NO-CH_4$	-0.2081×10^{-03}	0.9954×10^{-03}	$-0.2406\times10^{+00}$	$-0.2407\times10^{+00}$	1.4084	Present study
NO–He	$-0.3737\times10^{+19}$	0.3525×10^{-03}	$0.1059\times10^{+01}$	$-0.2464\times10^{+00}$	1.4581	Present study
NO–Ar	$-0.1512\times10^{+06}$	$0.2509\times10^{+00}$	$0.2360\times10^{+00}$	$-0.1107\times10^{+00}$	1.4030	Ref. 15
NO–N	$-0.3643\times10^{+02}$	0.5215×10^{-01}	0.2055×10^{-01}	$-0.1497\times10^{+00}$	1.5920	Ref. 26
NO–O	$-0.6880\times10^{+02}$	0.8767×10^{-01}	0.4601×10^{-01}	$-0.1328\times10^{+00}$	1.4987	Ref. 26

Downloaded 19 Apr 2011 to 143.248.103.97. Redistribution subject to AIP license or copyright; see http://pof.aip.org/about/rights_and_permissions

TABLE I. (*Continued.*)

Species	C_1	C_2	ω_1	ω_2	α	Source
NO–C	0.1918×10^{-07}	0.3580×10^{-06}	$-0.4095\times10^{+00}$	$-0.4095\times10^{+00}$	1.5796	Ref. 24
NO–H	$-0.1600\times10^{+15}$	0.7200×10^{-06}	$0.8229\times10^{+00}$	$-0.3901\times10^{+00}$	1.5823	Ref. 24
NO–N_2^+	0.8194×10^{-09}	0.1001×10^{-05}	$0.1680\times10^{+00}$	$-0.4000\times10^{+00}$	1.1039	Ref. 27
NO–O_2^+	$0.1693\times10^{+00}$	0.3121×10^{-20}	$-0.1065\times10^{+00}$	$-0.1128\times10^{+01}$	1.6952	Ref. 27
NO–NO^+	$0.1045\times10^{+10}$	0.1154×10^{-01}	$0.4442\times10^{+00}$	$-0.1930\times10^{+00}$	0.2491	Ref. 22
NO–N^+	0.8194×10^{-09}	0.1001×10^{-05}	$0.1680\times10^{+00}$	$-0.4000\times10^{+00}$	1.1039	Ref. 27
NO–O^+	0.8194×10^{-09}	0.1001×10^{-05}	$0.1680\times10^{+00}$	$-0.4000\times10^{+00}$	1.1039	Ref. 27
NO–C^+	$-0.4909\times10^{+30}$	0.1289×10^{-05}	$0.1682\times10^{+01}$	$-0.3945\times10^{+00}$	1.1097	Ref. 24
NO–H^+	$-0.4910\times10^{+30}$	0.1289×10^{-05}	$0.1682\times10^{+01}$	$-0.3945\times10^{+00}$	1.1097	Ref. 24
CO–CO	-0.1694×10^{-03}	0.1381×10^{-02}	$-0.2310\times10^{+00}$	$-0.2314\times10^{+00}$	2.8235	Present study
CO–CO_2	0.1461×10^{-02}	0.1233×10^{-25}	$-0.2274\times10^{+00}$	$-0.1380\times10^{+01}$	1.3812	Present study
CO–C_2	0.7370×10^{-03}	-0.2083×10^{-66}	$-0.2421\times10^{+00}$	$-0.3383\times10^{+01}$	1.4183	Present study
CO–H_2	0.4686×10^{-03}	$0.0000\times10^{+00}$	$-0.2449\times10^{+00}$	$0.0000\times10^{+00}$	1.4187	Present study
CO–CN	-0.2233×10^{-04}	0.9801×10^{-01}	$-0.2443\times10^{+00}$	$-0.1253\times10^{+00}$	1.1813	Present study
CO–CH_4	-0.2275×10^{-04}	0.8218×10^{-03}	$-0.2410\times10^{+00}$	$-0.2409\times10^{+00}$	1.4095	Present study
CO–He	$-0.2754\times10^{+07}$	0.1445×10^{-05}	$0.3604\times10^{+00}$	$-0.3720\times10^{+00}$	1.6121	Present study
CO–Ar	-0.2577×10^{-03}	0.9436×10^{-03}	$-0.2414\times10^{+00}$	$-0.2414\times10^{+00}$	1.4110	Present study
CO–N	$-0.2531\times10^{+16}$	0.9027×10^{-06}	$0.8957\times10^{+00}$	$-0.3919\times10^{+00}$	1.5687	Ref. 24
CO–O	$-0.2795\times10^{+34}$	0.7892×10^{-06}	$0.1936\times10^{+01}$	$-0.3958\times10^{+00}$	1.5620	Ref. 24
CO–C	$-0.1221\times10^{+18}$	0.8423×10^{-06}	$0.9797\times10^{+00}$	$-0.3919\times10^{+00}$	1.5867	Ref. 24
CO–H	$-0.1231\times10^{+14}$	0.7712×10^{-06}	$0.7587\times10^{+00}$	$-0.3893\times10^{+00}$	1.5810	Ref. 24
CO–N_2^+	$-0.4910\times10^{+30}$	0.1289×10^{-05}	$0.1682\times10^{+01}$	$-0.3945\times10^{+00}$	1.1097	Ref. 24
CO–NO^+	$-0.4908\times10^{+30}$	0.1289×10^{-05}	$0.1682\times10^{+01}$	$-0.3945\times10^{+00}$	1.1097	Ref. 24
CO–N^+	$-0.4910\times10^{+30}$	0.1289×10^{-05}	$0.1682\times10^{+01}$	$-0.3945\times10^{+00}$	1.1097	Ref. 24
CO–O^+	$-0.4910\times10^{+30}$	0.1289×10^{-05}	$0.1682\times10^{+01}$	$-0.3945\times10^{+00}$	1.1097	Ref. 24
CO–C^+	$-0.4910\times10^{+30}$	0.1289×10^{-05}	$0.1682\times10^{+01}$	$-0.3945\times10^{+00}$	1.1097	Ref. 24
CO–H+	$-0.4910\times10^{+30}$	0.1289×10^{-05}	$0.1682\times10^{+01}$	$-0.3945\times10^{+00}$	1.1097	Ref. 24
CO_2–CO_2	-0.1038×10^{-07}	0.9581×10^{-06}	$-0.3981\times10^{+00}$	$-0.3981\times10^{+00}$	1.5401	Present study
CO_2–C_2	0.1256×10^{-02}	0.4201×10^{-26}	$-0.2327\times10^{+00}$	$-0.1375\times10^{+01}$	1.4091	Present study
CO_2–H_2	-0.3005×10^{-03}	0.9183×10^{-03}	$-0.2423\times10^{+00}$	$-0.2423\times10^{+00}$	1.4136	Present study
CO_2–CN	0.1171×10^{-02}	0.2001×10^{-28}	$-0.2340\times10^{+00}$	$-0.1491\times10^{+01}$	1.4100	Present study
CO_2–CH_4	0.2280×10^{-02}	0.1524×10^{-16}	$-0.2188\times10^{+00}$	$-0.9011\times10^{+00}$	1.4001	Present study
CO_2–He	$-0.3997\times10^{+07}$	0.1422×10^{-05}	$0.3729\times10^{+00}$	$-0.3759\times10^{+00}$	1.5987	Present study
CO_2–Ar	-0.1630×10^{-03}	0.1018×10^{-02}	$-0.2397\times10^{+00}$	$-0.2397\times10^{+00}$	1.4033	Present study
CO_2–N	0.5030×10^{-07}	0.5853×10^{-06}	$-0.4007\times10^{+00}$	$-0.4006\times10^{+00}$	1.5621	Present study
CO_2–O	$-0.2372\times10^{+59}$	0.5325×10^{-03}	$0.3363\times10^{+01}$	$-0.2469\times10^{+00}$	1.4333	Present study
CO_2–C	-0.2872×10^{-13}	0.9653×10^{-07}	$-0.7533\times10^{+00}$	$-0.4502\times10^{+00}$	1.5750	Present study
CO_2–H	$-0.5419\times10^{+09}$	0.9815×10^{-06}	$0.5144\times10^{+00}$	$-0.3868\times10^{+00}$	1.5709	Present study
C_2–C_2	$-0.1310\times10^{+09}$	0.1417×10^{-05}	$0.4686\times10^{+00}$	$-0.3853\times10^{+00}$	1.5734	Present study
C_2–H_2	-0.2808×10^{-03}	0.7216×10^{-03}	$-0.2481\times10^{+00}$	$-0.2481\times10^{+00}$	1.4205	Present study
C_2–CN	0.6665×10^{-03}	$0.0000\times10^{+00}$	$-0.2455\times10^{+00}$	$0.0000\times10^{+00}$	1.4191	Present study
C_2–CH_4	-0.3582×10^{-04}	0.8297×10^{-03}	$-0.2425\times10^{+00}$	$-0.2425\times10^{+00}$	1.4144	Present study
C_2–He	$-0.2023\times10^{+07}$	0.1794×10^{-05}	$0.3464\times10^{+00}$	$-0.3690\times10^{+00}$	1.6206	Present study
C_2–Ar	0.7515×10^{-03}	0.5159×10^{-59}	$-0.2407\times10^{+00}$	$-0.2963\times10^{+01}$	1.4165	Present study
C_2–N	$-0.2074\times10^{+14}$	0.9486×10^{-06}	$0.7731\times10^{+00}$	$-0.3905\times10^{+00}$	1.5717	Ref. 24
C_2–O	$-0.7327\times10^{+22}$	0.8361×10^{-06}	$0.1271\times10^{+01}$	$-0.3942\times10^{+00}$	1.5641	Ref. 24
C_2–C	0.9473×10^{-08}	0.3466×10^{-06}	$-0.4109\times10^{+00}$	$-0.4112\times10^{+00}$	1.5822	Ref. 24
C_2–H	$-0.6225\times10^{+12}$	0.8125×10^{-06}	$0.6818\times10^{+00}$	$-0.3878\times10^{+00}$	1.5843	Ref. 24
C_2–N_2^+	$-0.4910\times10^{+30}$	$0.1289\times10^{+00}$	$0.1682\times10^{+01}$	$-0.3945\times10^{+00}$	1.1097	Ref. 24
C_2–NO^+	$-0.4910\times10^{+30}$	0.1289×10^{-05}	$0.1682\times10^{+01}$	$-0.3945\times10^{+00}$	1.1097	Ref. 24
C_2–N^+	$-0.4910\times10^{+30}$	0.1289×10^{-05}	$0.1682\times10^{+01}$	$-0.3945\times10^{+00}$	1.1097	Ref. 24
C_2–O^+	$-0.4910\times10^{+30}$	0.1289×10^{-05}	$0.1682\times10^{+01}$	$-0.3945\times10^{+00}$	1.1097	Ref. 24
C_2–C^+	$-0.1323\times10^{+12}$	0.1203×10^{-05}	$0.6317\times10^{+00}$	$-0.3865\times10^{+12}$	1.5890	Ref. 24
C_2–H^+	$-0.3174\times10^{+13}$	0.1089×10^{-05}	$0.7145\times10^{+00}$	$-0.3884\times10^{+00}$	1.5848	Ref. 24
H_2–H_2	$-0.2546\times10^{+04}$	$0.1368\times10^{+01}$	$0.1177\times10^{+00}$	-0.7133×10^{-01}	2.1811	Ref. 24

Downloaded 19 Apr 2011 to 143.248.103.97. Redistribution subject to AIP license or copyright; see http://pof.aip.org/about/rights_and_permissions

TABLE I. (*Continued.*)

Species	C_1	C_2	ω_1	ω_2	α	Source
H_2-CN	$-0.4176\times10^{+61}$	0.4594×10^{-03}	$0.3497\times10^{+01}$	$-0.2468\times10^{+00}$	1.4326	Present study
H_2-CH_4	-0.2694×10^{-03}	0.8041×10^{-03}	$-0.2443\times10^{+00}$	$-0.2443\times10^{+00}$	1.4184	Present study
H_2-He	$-0.1090\times10^{+07}$	0.1364×10^{-05}	$0.3372\times10^{+00}$	$-0.3666\times10^{+00}$	1.6279	Present study
H_2-Ar	$-0.9771\times10^{+09}$	0.8335×10^{-06}	$0.5338\times10^{+00}$	$-0.3874\times10^{+00}$	1.5698	Present study
H_2-N	$-0.1553\times10^{+08}$	0.1032×10^{-05}	$0.4168\times10^{+00}$	$-0.3800\times10^{+00}$	1.5890	Ref. 13
H_2-O	$-0.3563\times10^{+15}$	0.7371×10^{-06}	$0.8517\times10^{+00}$	$-0.3915\times10^{+00}$	1.5692	Ref. 24
H_2-C	$-0.2018\times10^{+10}$	0.9581×10^{-06}	$0.5320\times10^{+00}$	$-0.3832\times10^{+00}$	1.5952	Ref. 24
H_2-H	-0.3541×10^{-05}	0.8041×10^{-06}	$-0.3774\times10^{+00}$	$-0.4161\times10^{+00}$	2.4981	Ref. 13
$H_2-N_2^+$	$-0.4910\times10^{+30}$	0.1289×10^{-05}	$0.1682\times10^{+01}$	$-0.3945\times10^{+00}$	1.1097	Ref. 24
H_2-NO^+	$-0.4909\times10^{+30}$	0.1289×10^{-05}	$0.1682\times10^{+01}$	$-0.3945\times10^{+00}$	1.1097	Ref. 24
H_2-N^+	$-0.4910\times10^{+30}$	0.1289×10^{-05}	$0.1682\times10^{+01}$	$-0.3945\times10^{+00}$	1.1097	Ref. 24
H_2-O^+	$-0.4909\times10^{+30}$	0.1289×10^{-05}	$0.1682\times10^{+01}$	$-0.3945\times10^{+00}$	1.1097	Ref. 24
H_2-C^+	$-0.4910\times10^{+30}$	0.1289×10^{-05}	$0.1682\times10^{+01}$	$-0.3945\times10^{+00}$	1.1097	Ref. 24
H_2-H^+	$-0.4910\times10^{+30}$	0.1289×10^{-05}	$0.1682\times10^{+01}$	$-0.3945\times10^{+00}$	1.1097	Ref. 24
CN–CN	0.2663×10^{-07}	0.5335×10^{-06}	$-0.4040\times10^{+00}$	$-0.4040\times10^{+00}$	1.5714	Present study
$CN-CH_4$	-0.7249×10^{-04}	0.8429×10^{-03}	$-0.2428\times10^{+00}$	$-0.2428\times10^{+00}$	1.4151	Present study
CN–He	$-0.2036\times10^{+07}$	0.1780×10^{-05}	$0.3465\times10^{+00}$	$-0.3687\times10^{+00}$	1.6219	Present study
CN–Ar	-0.1183×10^{-03}	0.7768×10^{-03}	$-0.2434\times10^{+00}$	$-0.2434\times10^{+00}$	1.4165	Present study
CN–N	$-0.7749\times10^{+13}$	0.9701×10^{-06}	$0.7474\times10^{+00}$	$-0.3901\times10^{+00}$	1.5727	Ref. 24
CN–O	$-0.1197\times10^{+21}$	0.8571×10^{-00}	$0.1167\times10^{+01}$	$-0.3937\times10^{+00}$	1.5650	Ref. 24
CN–C	0.6884×10^{-08}	0.3411×10^{-06}	$-0.4117\times10^{+00}$	$-0.4119\times10^{+00}$	1.5831	Ref. 24
CN–H	$-0.2072\times10^{+12}$	0.8400×10^{-06}	$0.6534\times10^{+00}$	$-0.3872\times10^{+00}$	1.5853	Ref. 24
CN–N2+	$-0.4909\times10^{+30}$	0.1289×10^{-05}	$0.1682\times10^{+01}$	$-0.3945\times10^{+00}$	1.1097	Ref. 24
$CN-NO^+$	$-0.4910\times10^{+30}$	0.1289×10^{-05}	$0.1682\times10^{+01}$	$-0.3945\times10^{+00}$	1.1097	Ref. 24
$CN-N^+$	$-0.4909\times10^{+30}$	0.1289×10^{-05}	$0.1682\times10^{+01}$	$-0.3945\times10^{+00}$	1.1097	Ref. 24
$CN-O^+$	$-0.4910\times10^{+30}$	0.1289×10^{-05}	$0.1682\times10^{+01}$	$-0.3945\times10^{+00}$	1.1097	Ref. 24
$CN-C^+$	$-0.4909\times10^{+30}$	0.1289×10^{-05}	$0.1682\times10^{+01}$	$-0.3945\times10^{+00}$	1.1097	Ref. 24
$CN-H^+$	$-0.4910\times10^{+30}$	0.1289×10^{-05}	$0.1682\times10^{+01}$	$-0.3945\times10^{+00}$	1.1097	Ref. 24
CH_4-CH_4	$-0.2627\times10^{+54}$	0.9210×10^{-06}	$0.3093\times10^{+01}$	$-0.3963\times10^{+00}$	1.5532	Present study
CH_4-He	$-0.1823\times10^{+07}$	0.1560×10^{-05}	$0.3500\times10^{+00}$	$-0.3726\times10^{+00}$	1.6065	Present study
CH_4-Ar	-0.1393×10^{-03}	0.9225×10^{-03}	$-0.2405\times10^{+00}$	$-0.2405\times10^{+00}$	1.4079	Present study
CH_4-N	-0.7594×10^{-41}	0.4505×10^{-06}	$-0.2103\times10^{+01}$	$-0.4075\times10^{+00}$	1.5662	Present study
CH_4-O	$-0.8347\times10^{+07}$	0.1454×10^{-05}	$0.3937\times10^{+00}$	$-0.3795\times10^{+00}$	1.5877	Present study
CH_4-C	-0.8642×10^{-21}	0.1964×10^{-06}	$-0.1110\times10^{+01}$	$-0.4296\times10^{+00}$	1.5800	Present study
CH_4-H	$-0.3962\times10^{+11}$	0.9103×10^{-06}	$0.6189\times10^{+00}$	$-0.3872\times10^{+00}$	1.5764	Present study
He–He	$-0.1367\times10^{+05}$	0.4081×10^{-05}	$0.2125\times10^{+00}$	$-0.3388\times10^{+00}$	1.6804	Present study
He–Ar	$-0.2176\times10^{+07}$	0.1345×10^{-05}	$0.3572\times10^{+00}$	$-0.3724\times10^{+00}$	1.6091	Present study
He–N	$-0.2572\times10^{+02}$	$0.3444\times10^{+01}$	-0.1326×10^{-01}	-0.6528×10^{-01}	1.5359	Ref. 16
He–O	$-0.1384\times10^{+03}$	$0.3741\times10^{+00}$	0.5708×10^{-01}	-0.9533×10^{-01}	1.5202	Ref. 16
He–C	$-0.4878\times10^{+03}$	$0.1823\times10^{+00}$	0.8754×10^{-01}	$-0.1128\times10^{+00}$	1.5823	Ref. 16
He–H	$-0.1425\times10^{+13}$	0.6660×10^{-03}	$0.6786\times10^{+00}$	$-0.2237\times10^{+00}$	1.4722	Present study
Ar–Ar	$-0.6469\times10^{+05}$	$0.2649\times10^{+00}$	$0.2147\times10^{+00}$	$-0.1092\times10^{+00}$	1.4126	Ref. 15
Ar–N	$-0.6090\times10^{+02}$	0.3308×10^{-01}	0.4400×10^{-01}	$-0.1553\times10^{+00}$	1.5596	Ref. 25
Ar–O	$-0.1668\times10^{+03}$	0.6715×10^{-01}	0.6912×10^{-01}	$-0.1405\times10^{+00}$	1.5026	Ref. 19
Ar–C	$-0.2439\times10^{+09}$	0.2673×10^{-05}	$0.4776\times10^{+00}$	$-0.3654\times10^{+00}$	1.5724	Present study
Ar–H	$-0.4676\times10^{+10}$	0.1616×10^{-05}	$0.5662\times10^{+00}$	$-0.3701\times10^{+00}$	1.5646	Present study
N–N	$-0.1186\times10^{+03}$	$0.7881\times10^{+02}$	-0.2576×10^{-01}	-0.3624×10^{-01}	1.5044	Ref. 7
N–O	$-0.2860\times10^{+03}$	$0.2194\times10^{+00}$	0.6906×10^{-01}	$-0.1148\times10^{+00}$	1.5605	Ref. 7
N–C	$-0.2234\times10^{+18}$	0.4962×10^{-02}	$0.9460\times10^{+00}$	$-0.1886\times10^{+00}$	1.6003	Ref. 14
N–H	$-0.4098\times10^{+02}$	$0.1089\times10^{+02}$	-0.3046×10^{-01}	-0.6337×10^{-01}	1.4537	Ref. 10
$N-N_2^+$	0.8194×10^{-09}	0.1001×10^{-05}	$0.1680\times10^{+00}$	$-0.4000\times10^{+00}$	1.1039	Ref. 27
$N-O_2^+$	0.3835×10^{-01}	0.1007×10^{-22}	$-0.1403\times10^{+00}$	$-0.1242\times10^{+01}$	1.5795	Ref. 27
$N-NO^+$	0.8194×10^{-09}	0.1001×10^{-05}	$0.1680\times10^{+00}$	$-0.4000\times10^{+00}$	1.1039	Ref. 27
$N-N^+$	$0.3682\times10^{+00}$	-0.4143×10^{-26}	$-0.1143\times10^{+00}$	$-0.1295\times10^{+02}$	0.1599	Ref. 17
$N-O^+$	$-0.6657\times10^{+01}$	$0.4563\times10^{+01}$	$-0.1093\times10^{+00}$	$-0.1188\times10^{+00}$	1.3899	Ref. 17

Downloaded 19 Apr 2011 to 143.248.103.97. Redistribution subject to AIP license or copyright; see http://pof.aip.org/about/rights_and_permissions

TABLE I. (*Continued.*)

Species	C_1	C_2	ω_1	ω_2	α	Source
N–C^+	$-0.4910\times10^{+30}$	0.1289×10^{-05}	$0.1682\times10^{+01}$	$-0.3945\times10^{+00}$	1.1097	Ref. 24
N–H^+	$-0.4910\times10^{+30}$	0.1289×10^{-05}	$0.1682\times10^{+01}$	$-0.3945\times10^{+00}$	1.1097	Ref. 24
O–O	$-0.7504\times10^{+07}$	0.3340×10^{-03}	$0.3642\times10^{+00}$	$-0.2498\times10^{+00}$	1.5917	Ref. 7
O–C	$-0.4054\times10^{+02}$	$0.3339\times10^{+02}$	-0.6234×10^{-01}	-0.6745×10^{-01}	1.5108	Ref. 14
O–H	$-0.2618\times10^{+11}$	0.8157×10^{-06}	$0.6071\times10^{+00}$	$-0.3872\times10^{+00}$	1.5789	Ref. 24
O–N_2^+	-0.8194×10^{-09}	0.1001×10^{-05}	$0.1680\times10^{+00}$	$-0.4000\times10^{+00}$	1.1039	Ref. 27
O–O_2^+	0.1118×10^{-01}	0.2544×10^{-24}	$-0.1668\times10^{+00}$	$-0.1315\times10^{+01}$	1.5527	Ref. 27
O–NO^+	0.8194×10^{-09}	0.1001×10^{-05}	$0.1680\times10^{+00}$	$-0.4000\times10^{+00}$	1.1039	Ref. 27
O–N^+	-0.4193×10^{-15}	0.2931×10^{-11}	$-0.8873\times10^{+00}$	$-0.6998\times10^{+00}$	1.5091	Ref. 18
O–O^+	$0.5345\times10^{+00}$	-0.2956×10^{-77}	$-0.1007\times10^{+00}$	$-0.3881\times10^{+01}$	0.1676	Ref. 17
O–C^+	$-0.4909\times10^{+30}$	0.1289×10^{-05}	$0.1682\times10^{+01}$	$-0.3945\times10^{+00}$	1.1097	Ref. 24
O–H^+	$-0.4909\times10^{+30}$	0.1289×10^{-05}	$0.1682\times10^{+01}$	$-0.3945\times10^{+00}$	1.1097	Ref. 24
C–C	$-0.2975\times10^{+05}$	$0.3118\times10^{+00}$	$0.1811\times10^{+00}$	$-0.1073\times10^{+00}$	1.5993	Ref. 14
C–H	-0.1837×10^{-24}	0.5417×10^{-07}	$-0.1308\times10^{+01}$	$-0.4557\times10^{+00}$	1.5931	Ref. 24
C–N_2^+	$-0.4910\times10^{+30}$	0.1289×10^{-05}	$0.1682\times10^{+01}$	$-0.3945\times10^{+00}$	1.1097	Ref. 24
C–NO^+	$-0.4910\times10^{+30}$	0.1289×10^{-05}	$0.1682\times10^{+01}$	$-0.3945\times10^{+00}$	1.1097	Ref. 24
C–N^+	$-0.4910\times10^{+30}$	0.1289×10^{-05}	$0.1682\times10^{+01}$	$-0.3945\times10^{+00}$	1.1097	Ref. 24
C–O^+	$-0.4910\times10^{+30}$	0.1289×10^{-05}	$0.1682\times10^{+01}$	$-0.3945\times10^{+00}$	1.1097	Ref. 24
C–C^+	$-0.4910\times10^{+30}$	0.1289×10^{-30}	$0.1682\times10^{+01}$	$-0.3945\times10^{+00}$	1.1097	Ref. 24
C–H^+	$-0.4910\times10^{+30}$	0.1289×10^{-05}	$0.1682\times10^{+01}$	$-0.3945\times10^{+00}$	1.1097	Ref. 24
H–H	-0.8398×10^{-13}	0.1588×10^{-11}	$-0.7873\times10^{+00}$	$-0.7244\times10^{+00}$	1.6772	Ref. 24
H–N_2^+	$-0.4910\times10^{+30}$	0.1289×10^{-05}	$0.1682\times10^{+01}$	$-0.3945\times10^{+00}$	1.1097	Ref. 24
H–NO^+	$-0.4910\times10^{+30}$	0.1289×10^{-05}	$0.1682\times10^{+01}$	$-0.3945\times10^{+00}$	1.1097	Ref. 24
H–N^+	$-0.4910\times10^{+30}$	0.1289×10^{-05}	$0.1682\times10^{+01}$	$-0.3945\times10^{+00}$	1.1097	Ref. 24
H–O^+	$-0.4909\times10^{+30}$	0.1289×10^{-05}	$0.1682\times10^{+01}$	$-0.3945\times10^{+00}$	1.1097	Ref. 24
H–C^+	$-0.4910\times10^{+30}$	0.1289×10^{-05}	$0.1682\times10^{+01}$	$-0.3945\times10^{+00}$	1.1097	Ref. 24
H–H^+	$-0.1279\times10^{+18}$	0.9806×10^{-09}	$0.9161\times10^{+00}$	$-0.5724\times10^{+00}$	0.4255	Ref. 24

Ar–Ar collision are compared with other results based on the VSS and GSS models and the reference values obtained by the *ab initio* calculations.[14] Because the LJ potential is comparatively adequate to describe the molecular interaction for noble gases, such as Ar species, and the collision parameters of the VSS model were calculated from the LJ potential, the discrepancy between the reference values and the transport properties of the VSS model was relatively small. However, even though the collision parameters of the GSS model were calculated from the LJ potential, the transport properties of the GSS model were significantly different from the refer-

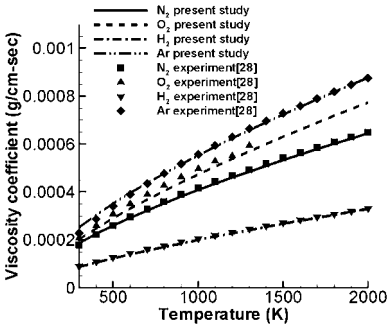

FIG. 4. Comparison of viscosity coefficients between the present study and experiment (Ref. 28).

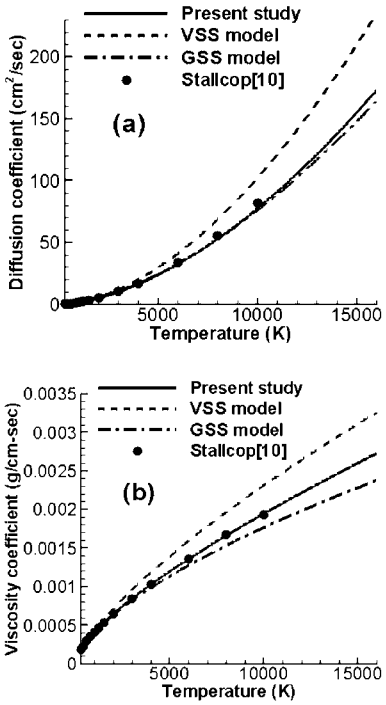

FIG. 5. Comparison of the transport properties for N_2–N_2 collisions between the present study and the VSS model, the GSS model, and the reference values obtained from the *ab initio* calculations (Ref. 10). (a) Diffusion coefficient; (b) viscosity coefficient.

Downloaded 19 Apr 2011 to 143.248.103.97. Redistribution subject to AIP license or copyright; see http://pof.aip.org/about/rights_and_permissions

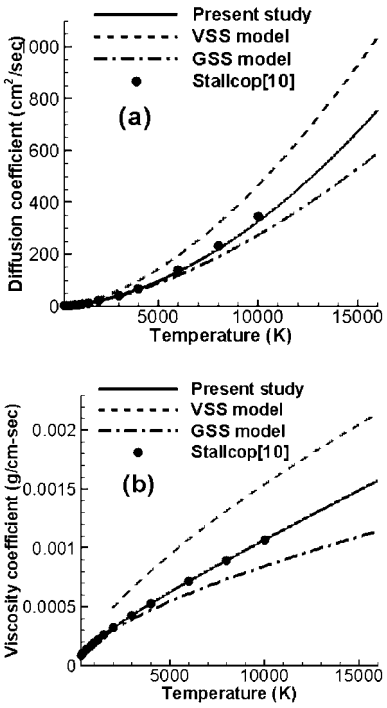

FIG. 6. Comparison of the transport properties for N_2–H_2 collisions between the present study and the VSS model, the GSS model, and the reference values obtained by the *ab initio* calculations (Ref. 10). (a) Diffusion coefficient; (b) viscosity coefficient.

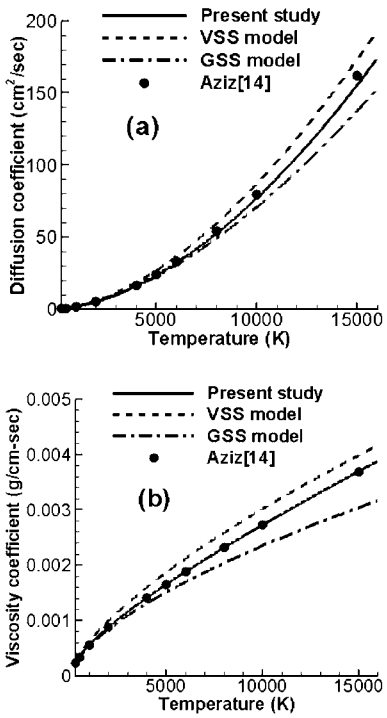

FIG. 8. Comparison of the transport properties for Ar–Ar collisions between the present study and the VSS model, the GSS model, and the reference values obtained by the *ab initio* calculations (Ref. 14). (a) Diffusion coefficient; (b) viscosity coefficient.

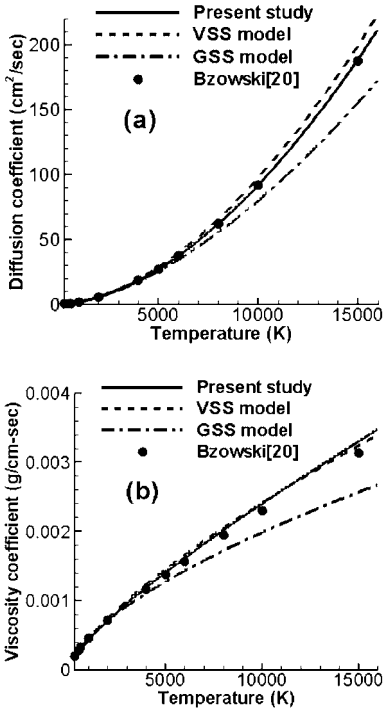

FIG. 7. Comparison of the transport properties for NO–NO collisions between the present study and the VSS model, the GSS model, and the reference values obtained by the theoretical data (Ref. 20). (a) Diffusion coefficient; (b) viscosity coefficient.

ence values. This is because a constant set of the scattering parameters was used in the GSS model.

For the collision pairs of molecule-atom and atom-atom, the transport properties by the present study were validated by comparing the results with the reference transport properties obtained by the *ab initio* calculations.[7,11] Comparison with previous elastic collision models is not possible, because the collision parameters of the VSS and GSS models do not exist for these collision pairs.

In Fig. 9, the transport properties for N–O, N_2–N, O_2–H, and H_2-N collisions obtained by the present study were compared with the reference values from the *ab initio* calculations.[7,11] It shows that the present results agree well with the reference values. While it is known that the elastic collisions between molecule-atom and atom-atom are not well described by the GSS model, these elastic collisions were well simulated by adopting the new collision parameters obtained in the present study.

In the case of the charged particles, the collisions are classified as either resonant or nonresonant. In Fig. 10, the transport properties obtained by the present study by accounting for the resonant effect of the $N–N^+$, $O–O^+$, $N_2–N_2^+$, and $NO–NO^+$ collisions were compared with the reference values calculated from the *ab initio* calculations[16] and the theoretical data.[21,22] The theoretical data were calculated by using the charge transfer cross section and the polarizability model. It shows that the transport properties obtained by the present study agree well with the reference values.

For the nonresonant collisions, the transport properties

Downloaded 19 Apr 2011 to 143.248.103.97. Redistribution subject to AIP license or copyright; see http://pof.aip.org/about/rights_and_permissions

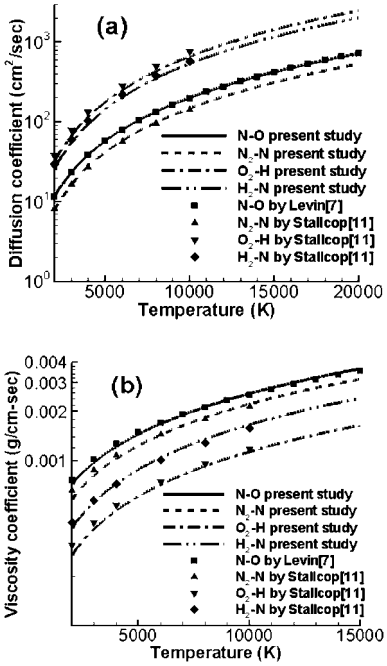

FIG. 9. Comparison of the transport properties for diatom-atom and atom-atom collisions between the present study and the reference values obtained by the *ab initio* calculations (Refs. 7 and 11). (a) Diffusion coefficient; (b) viscosity coefficient.

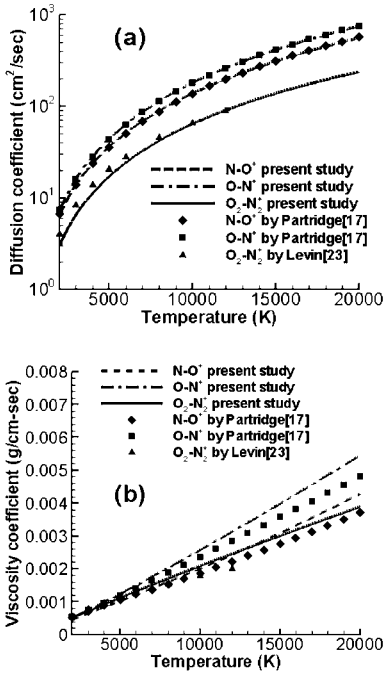

FIG. 11. Comparison of the transport properties for the nonresonant collisions between the present study and the reference values obtained by the *ab initio* calculations (Ref. 17) and the compilation (Ref. 23). (a) Diffusion coefficient; (b) viscosity coefficient.

obtained by the present study for the $O_2-N_2^+$, $N-O^+$, and $O-N^+$ collisions were compared with the reference values obtained by the *ab initio* calculations[17] and the compilation.[23] The collision integrals of the compilation[23] were calculated based on the modified Tang and Toennies potential.[29] The results in Fig. 11 show that the transport properties obtained by the present study agree well with the reference values.

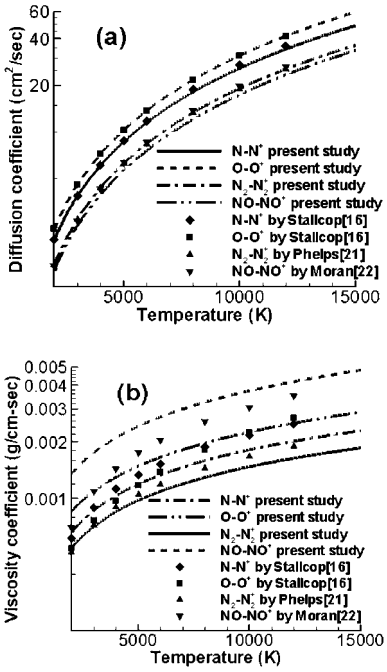

FIG. 10. Comparison of the transport properties for the resonant collisions between the present study and the reference values obtained by the *ab initio* calculations (Ref. 16) and the theoretical data (Refs. 21 and 22). (a) Diffusion coefficient; (b) viscosity coefficient.

V. SAMPLE DSMC CALCULATIONS

In order to examine the effect of the modification of the GSS model, sample DSMC calculations were performed for flow around a circular cylinder. The two selected freestream velocities were 5 km/s and 8 km/s, and the Knudsen number based on the cylinder diameter was set to 0.1. The fluid was composed of N_2 and NO species, and the temperature of the freestream flow was set to 300 K. For the purpose of verifying the effect of the elastic collision model, inelastic collisions were excluded from the calculations. The results based on the new collision parameters obtained in the present study were compared with those of the previous elastic collision models.

In Fig. 12, the translational temperature contours for N_2 species are compared between the present study and the GSS and VSS models. It shows that the contour of the highest temperature by the present study (level 5 in the figure) elongated further downstream than that of the VSS model for both freestream velocity cases. In the case of the low temperature contours, the results of the VSS model expanded further away from the cylinder than those of the present study. This is caused by the difference in the collision parameters and the transport properties between the present study and the VSS model as shown in Fig. 5.

In Fig. 13, the translational temperature distributions along the stagnation streamline are compared. It shows that

Downloaded 19 Apr 2011 to 143.248.103.97. Redistribution subject to AIP license or copyright; see http://pof.aip.org/about/rights_and_permissions

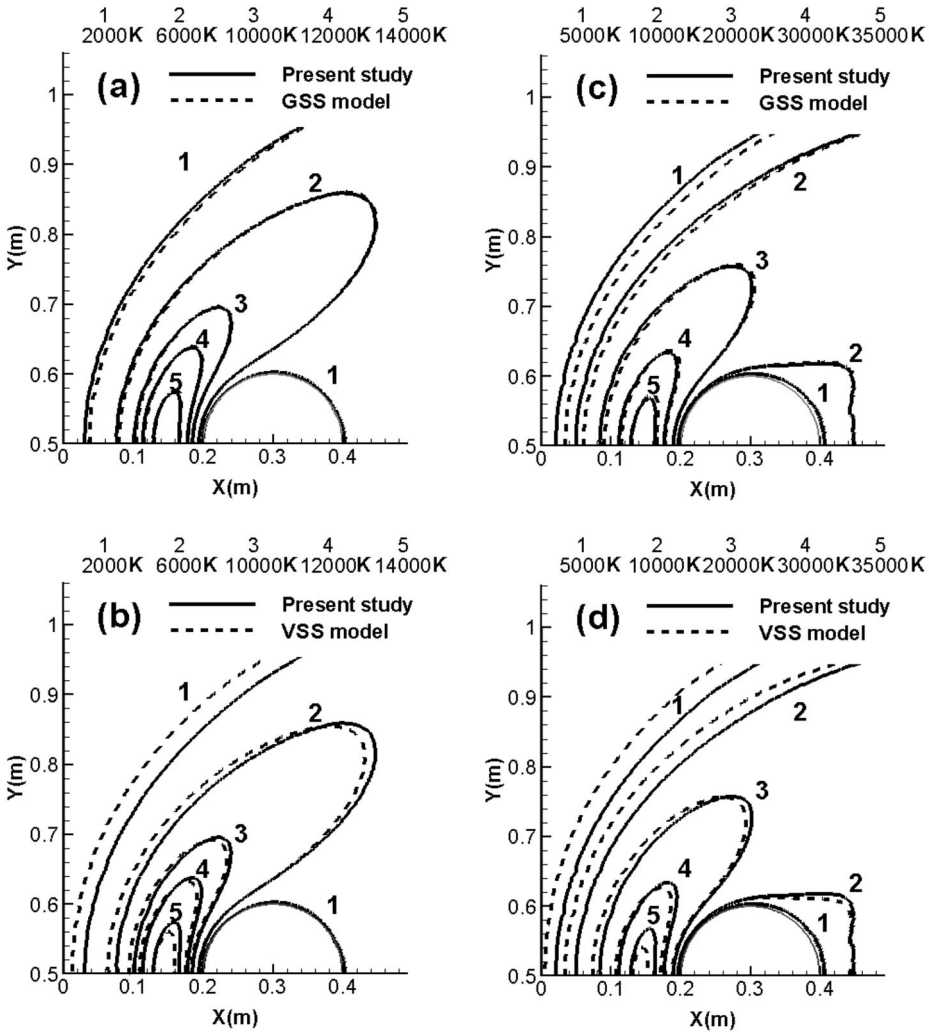

FIG. 12. Translational temperature contours for N_2 species for flow around a circular cylinder. (a) Comparison with the GSS model at 5 km/s freestream velocity. (b) Comparison with the VSS model at 5 km/s freestream velocity. (c) Comparison with the GSS model at 8 km/s freestream velocity. (d) Comparison with the VSS model at 8 km/s freestream velocity.

the maximum translational temperatures obtained based on the present study were approximately 500 K and 2000 K degrees higher than those of the VSS model for each freestream velocity case, respectively. This temperature difference may affect the chemical reaction significantly by changing the probability of the inelastic collision and the collision energy. It also indicated that the effect of the new collision parameters obtained in the present study was more evident when the freestream velocity increased. However, in the case of the GSS model, the difference of the translational temperature from the present study was smaller than that of the VSS model, because the discrepancy of the transport properties of the GSS model was less than that for the VSS model. It is believed that the results by the present study are more accurate than those of the VSS and GSS models, since the transport properties of the collision parameters by the present study are in better agreement with the reference values as shown in Fig. 5.

In Fig. 14, the heat flux and pressure distributions along the cylinder surface from the leading-edge stagnation point to the trailing-edge stagnation point are compared between the present study and the VSS model for N_2 species at 8 km/s freestream velocity. The pressure was normalized by the freestream value. It shows that the heat flux at the

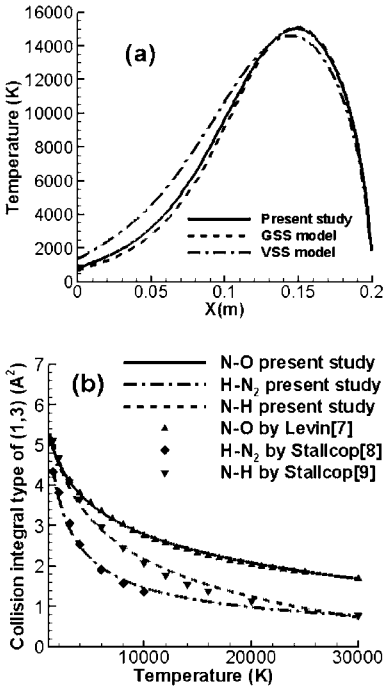

FIG. 13. Comparison of the translational temperature for N_2 species along the stagnation streamline between the present study and the GSS and VSS models for flow around a circular cylinder. (a) Freestream velocity at 5 km/s. (b) Freestream velocity at 8 km/s.

Downloaded 19 Apr 2011 to 143.248.103.97. Redistribution subject to AIP license or copyright; see http://pof.aip.org/about/rights_and_permissions

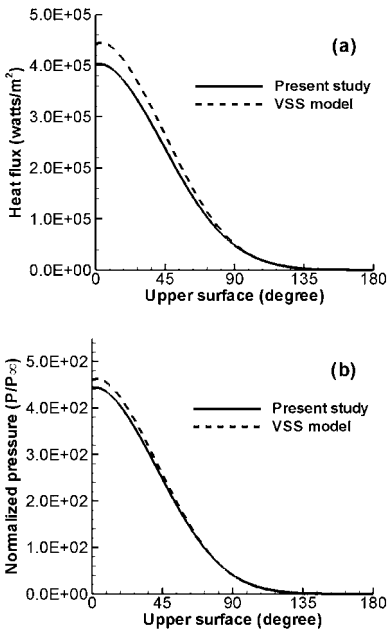

FIG. 14. Comparison of heat flux and normalized pressure distributions along the cylinder surface between the present study and the VSS model for N_2 species at 8 km/s freestream velocity. (a) Heat flux distribution; (b) normalized pressure distribution.

leading-edge stagnation point by the present study was 4.0×10^5 W/m^2, which was approximately 10% less than that of the VSS model. At the trailing-edge stagnation point, the relative difference between the two models increased to 38%, even though the magnitude of the heat flux was small compared to the leading-edge stagnation point. The difference of the normalized surface pressure between the two models at the leading-edge and trailing-edge stagnation points were approximately 6% and 40%, respectively. It was demonstrated that the substantial discrepancy of the transport properties between the present model and the VSS model for N_2 species shown in Fig. 5 resulted in fairly large changes of the surface properties in the DSMC simulations. It is expected that the effect of the present model on the surface properties is more significant as the gas flow becomes further rarefied, as shown at the cylinder trailing-edge region.

In Fig. 15, the translational temperature contours for NO species are compared between the present study and the GSS and VSS models. It shows that unlike the N_2 species, the high temperature region obtained by the present study was slightly smaller than that of the GSS model for both freestream velocity cases, while the low temperature region was expanded wider than that of the GSS model.

In Fig. 16, the translational temperature distributions

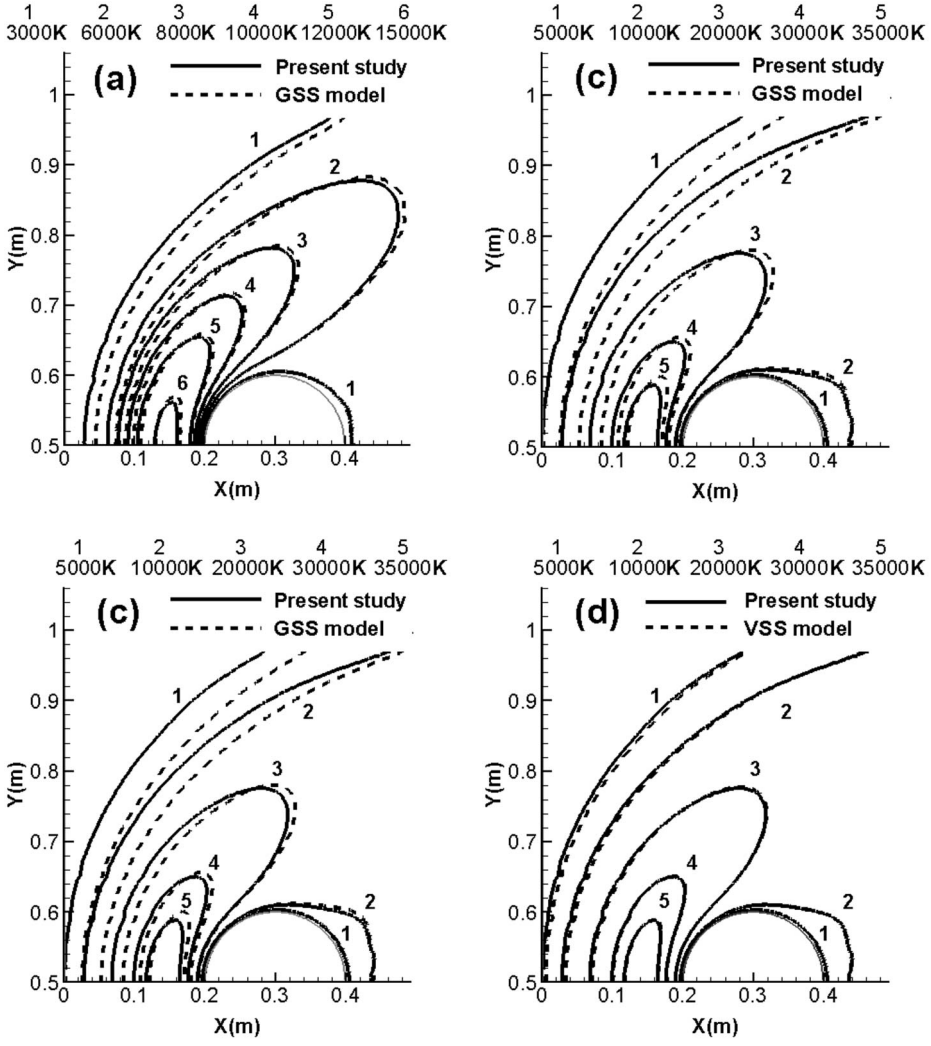

FIG. 15. Translational temperature contours for NO species for flow around a circular cylinder. (a) Comparison with the GSS model at 5 km/s freestream velocity. (b) Comparison with the VSS model at 5 km/s freestream velocity. (c) Comparison with the GSS model at 8 km/s freestream velocity. (d) Comparison with the VSS model at 8 km/s freestream velocity.

Downloaded 19 Apr 2011 to 143.248.103.97. Redistribution subject to AIP license or copyright; see http://pof.aip.org/about/rights_and_permissions

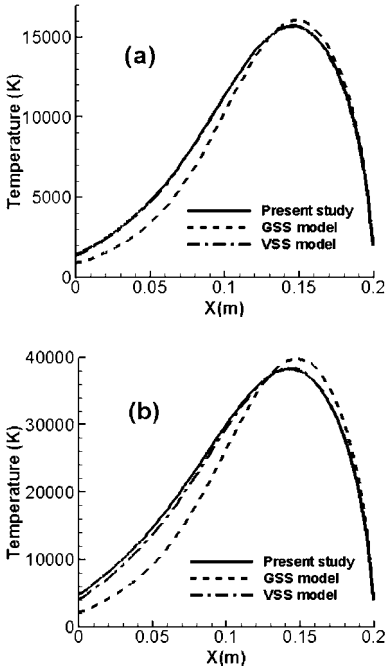

FIG. 16. Comparison of the translational temperature for NO species along the stagnation streamline between the present study and the GSS and VSS models for flow around a circular cylinder. (a) Freestream velocity at 5 km/s. (b) Freestream velocity at 8 km/s.

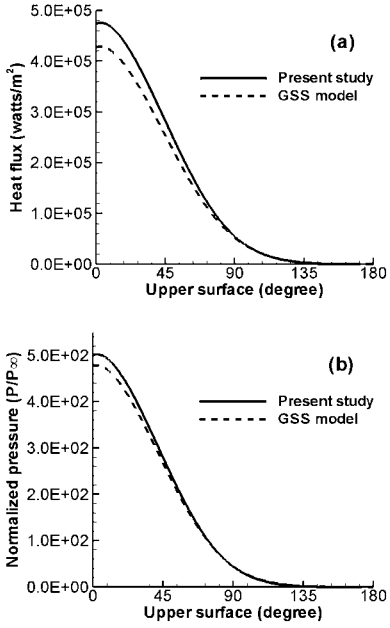

FIG. 17. Comparison of heat flux and normalized pressure distributions along the cylinder surface between the present study and the GSS model for NO species at 8 km/s freestream velocity. (a) Heat flux distribution; (b) normalized pressure distribution.

along the stagnation streamline are compared. It shows that the maximum translational temperature obtained by the present study was less than that of the GSS model, but the overall level of the translational temperature at the upstream of the maximum temperature location was higher than that of the GSS model. In the case of the VSS model, the contours of the translational temperature and its distribution along the stagnation streamline were similar to the present study, because the transport properties were almost identical as shown in Fig. 7.

In Fig. 17, the heat flux and normalized pressure distributions along the cylinder surface from the leading-edge stagnation point to the trailing-edge stagnation point are compared between the present study and the GSS model for NO species at 8 km/s freestream velocity. It shows that the heat flux at the leading-edge stagnation point by the present study was 4.8×10^5 W/m^2, approximately 10% higher than that of the GSS model. At the trailing-edge stagnation point, the difference of the heat flux between the two models increased to 55%. The increments of the normalized surface pressure at the leading-edge and trailing-edge stagnation points were approximately 6% and 68%, respectively, as a result of the different transport properties between the present model and the GSS model shown in Fig. 7.

Since the transport properties evaluated by the new collision parameters in the present study for the 191 collision pairs involving 22 species of neutral and charged particles were in better agreement with the reference values, it is believed that the DSMC calculations for the 191 collision pairs are more accurate than the previous elastic collision models.

VI. CONCLUDING REMARKS

A modification and an expansion of the general soft-sphere (GSS) model for elastic collisions were made for the purpose of attaining a higher accuracy in the DSMC calculations of hypersonic flows at high temperatures. The total cross section and the soft-sphere assumption of the GSS model were augmented by the implicitly species-dependent variable scattering parameters. The new collision parameters of the present study which were valid over the temperature range of 300–50 000 K were derived by using the diffusion and viscosity collision integrals simultaneously taken from experiments, the most recent data obtained through the *ab initio* calculations from quantum-mechanically derived potential energy surfaces, and the theoretical data. The new collision parameters were tabulated for 191 collision pairs involving 22 species. It was shown that the transport properties calculated by using the present collision parameters were much closer to the reference values derived from the most recent collision integrals by the Chapman–Enskog method than the existing elastic collision models. Sample DSMC calculations showed that a discernible difference exists in the results between the present study and the existing models.

[1] J. Fan, "A general soft-sphere model for Monte Carlo simulation," Phys. Fluids **14**, 4399 (2002).
[2] H. A. Hassan and D. B. Hash, "A generalized hard sphere model for Monte Carlo simulation," Phys. Fluids A **5**, 738 (1993).
[3] J. A. Kunc, D. B. Hash, and H. A. Hassan, "The GHS interaction model for strong attractive potentials," Phys. Fluids **7**, 1173 (1995).
[4] J. O. Hirschfelder, C. F. Curtiss, and R. B. Bird, *Molecular Theory of Gases and Liquids* (Wiley, New York, 1954).
[5] K. Koura and H. Matsumoto, "Variable soft sphere molecular model for inverse-power-law or Lennard-Jones potential," Phys. Fluids A **3**, 2459 (1991).

Downloaded 19 Apr 2011 to 143.248.103.97. Redistribution subject to AIP license or copyright; see http://pof.aip.org/about/rights_and_permissions

[6]K. Koura and H. Matsumoto, "Variable soft sphere molecular model for air species," Phys. Fluids A **4**, 1083 (1992).
[7]E. Levin, H. Partridge, and J. R. Stallcop, "Collision integrals and high temperature transport properties for N–N, O–O, and N–O," J. Thermophys. Heat Transfer **4**, 469 (1990).
[8]J. R. Stallcop, H. Partridge, S. P. Walch, and E. Levin, "H–N_2 interaction energies, transport cross sections, and collision integrals," J. Chem. Phys. **97**, 3431 (1992).
[9]J. R. Stallcop, C. W. Bauschlicher, and H. Partridge, "Theoretical study of hydrogen and nitrogen interactions: N–H transport cross sections and collision integrals," J. Chem. Phys. **97**, 5578 (1992).
[10]J. R. Stallcop, H. Partridge, and E. Levin, "Effective potential energies and transport cross sections for interactions of hydrogen and nitrogen," Phys. Rev. A **62**, 062709 (2000).
[11]J. R. Stallcop, H. Partridge, and E. Levin, "Effective potential energies and transport cross sections for atom-molecule interactions of nitrogen and oxygen," Phys. Rev. A **64**, 042722 (2001).
[12]J. R. Stallcop, H. Partridge, and E. Levin, "H–H_2 collision integrals and transport coefficients," Chem. Phys. Lett. **254**, 25 (1996).
[13]J. R. Stallcop, H. Partridge, A. Paradhan, and E. Levin, "Potential energies and collision integrals for interaction of carbon and nitrogen atoms," J. Thermophys. Heat Transfer **14**, 480 (2000).
[14]R. A. Aziz and M. J. Slaman, "The repulsive wall of the Ar–Ar interatomic potential reexamined," J. Chem. Phys. **92**, 1030 (1990).
[15]H. Partridge, J. R. Stallcop, and E. Levin, "Potential energy curves and transport properties for the interaction of He with other ground-state atoms," J. Chem. Phys. **115**, 6471 (2001).
[16]J. R. Stallcop and H. Partridge, "Resonance charge transfer, transport cross section, and collision integrals for $N^+(3P)$-N(4*S*0) and $O^+(4S0)$-O(3*P*) interactions," J. Chem. Phys. **95**, 6429 (1991).
[17]H. Partridge and J. R. Stallcop, "Transport cross sections and collision integrals for N(4*s*0)-$O^+(4S0)$ and $N^+(3P)$-O(3*O*) interactions," Chem. Phys. Lett. **184**, 505 (1991).
[18]S. J. Cubley and E. A. Mason, "Atom-molecule and molecule-molecule potentials and transport collision integrals for high temperature air species," Phys. Fluids **18**, 1109 (1975).
[19]A. B. Murphy and C. J. Arundell, "Transport coefficients of argon, nitrogen, oxygen, argon-nitrogen, and argon-oxygen plasmas," Plasma Chem. Plasma Process. **14**, 451 (1994).
[20]J. Bzowski, J. Kestine, E. A. Mason, and F. J. Uribe, "Equilibrium and transport properties of gaseous mixture at low density," J. Phys. Chem. Ref. Data **19**, 1179 (1990).
[21]A. V. Phelps, "Cross sections and swarm coefficients for nitrogen ions and neutrals in N_2 and argon ions and neutral in Ar for energies from 0.1 eV to 10 keV," J. Phys. Chem. Ref. Data **20**, 557 (1991).
[22]F. Moran, M. R. Flannery, and P. C. Cosby, "Molecular charged transfer. II. Experimental and theoretical investigation of the role of incident-ion vibrational states in O_2^+–O_2 and NO^+–NO collisions," J. Chem. Phys. **61**, 1261 (1974).
[23]E. Levin and M. J. Wright, "Collision integrals for ion-neutral interactions of nitrogen and oxygen," J. Thermophys. Heat Transfer **18**, 143 (2004).
[24]C. Park, R. L. Jaffe, and H. Partridge, "Chemical kinetic parameters of hyperbolic earth entry," J. Thermophys. Heat Transfer **15**, 76 (2001).
[25]M. J. Wright, D. Bose, G. E. Palmer, and E. Levin, "Recommended collision integrals for transport property computation, part 1: Air species," AIAA J. **43**, 2558 (2005).
[26]M. Capitelli, C. Gorse, S. Longo, and D. Giordano, "Collision integrals of high temperature air species," J. Thermophys. Heat Transfer **14**, 259 (2000).
[27]R. N. Gupta, J. M. Yos, R. A. Thompson, and K. Lee, "A review of reaction rates and thermodynamic and transport properties for an 11 species air model for chemical and thermal nonequilibrium calculations to 30,000 K," NASA Reference Publ. 1232, August 1990.
[28]G. S. Maitland and E. B. Smith, "Critical reassessment of viscosities of 11 common gases," J. Chem. Eng. Data **17**, 150 (1972).
[29]K. T. Tang and J. P. Toennies, "An improved simple model for the van der Waals potential based on universal damping functions for the dispersion coefficients," J. Chem. Phys. **80**, 3726 (1984).

Downloaded 19 Apr 2011 to 143.248.103.97. Redistribution subject to AIP license or copyright; see http://pof.aip.org/about/rights_and_permissions